Constraining Ganymede's neutral and plasma environments through simulations of its ionosphere and Galileo observations

Gianluca Carnielli, M. Galand, François Leblanc, Ronan Modolo, A. Beth, X. Jia

Manuscript Details

Manuscript number	ICARUS_2019_454_R1
Title	Constraining Ganymede's neutral and plasma environments through simulations of its ionosphere and Galileo observations
Article type	Research paper

Abstract

Ganymede's neutral and plasma environments are poorly constrained by observations. Carnielli et al. (2019) developed the first 3D ionospheric model aimed at understanding the dynamics of the present ion species and at quantifying the presence of each component in the moon's magnetosphere. The model outputs were compared with Galileo measurements of the ion energy flux, ion bulk velocity and electron number density made during the G2 flyby. A good agreement was found in terms of ion energy distribution and bulk velocity, but not in terms of electron number density. In this work, we present some improvements to our model Carnielli et al. (2019) and quantitatively address the possible sources of the discrepancy found in the electron number density between the Galileo observations and our ionospheric model. We have improved the ion model by developing a collision scheme to simulate the charge-exchange interaction between the exosphere and the ionosphere. We have simulated the energetic component of the O$_2$ population, which is missing in the exospheric model of Leblanc et al. (2017) and added it to the original distribution, hence improving its description at high altitudes. These improvements are found to be insufficient to explain the discrepancy in the electron number density. We provide arguments that the input O$_2$ exosphere is underestimated and that the plasma production acts asymmetrically between the Jovian and anti-Jovian hemispheres. In particular, we estimate that the O$_2$ column density should be greater than 10^{15}~cm^{-2}, i.e., higher than previously derived upper limits (and a factor 10 higher than the values from Leblanc et al. (2017)), and that the ionization frequency from electron impact must be higher in the anti-Jovian hemisphere for the G2 flyby conditions.

Keywords	Ganymede; Ionospheres; Jupiter; Satellites; Satellite Atmospheres

Corresponding Author	Gianluca Carnielli
Corresponding Author's Institution	Imperial College London
Order of Authors	Gianluca Carnielli, Marina Galand, Ronan MODOLO, Francois Leblanc, Arnaud Beth, Xianzhe jia
Suggested reviewers	Andrew Poppe, Benjamin Teolis, Christina Plainaki, Carol Paty, robert johnson

Submission Files Included in this PDF

File Name [File Type]

refereeAnswers.docx [Response to Reviewers]

Highlights.docx [Highlights]

manuscript.pdf [Manuscript File]

To view all the submission files, including those not included in the PDF, click on the manuscript title on your EVISE Homepage, then click 'Download zip file'.

Answers to referee's comments on the manuscript: Constraining Ganymede's neutral and plasma environments through simulations of its ionosphere and Galileo observations

G. Carnielli, M. Galand, F. Leblanc, R. Modolo, A. Beth, X. Jia

Preamble:

We would like to warmly thank both referees for their constructive comments, suggestions, and time devoted to review the manuscript. By considering all the comments received, we have updated our work. In blue are the original referee's comments, in red are our answers.

Reviewer 1:

This paper sheds new light on the Ganymede gas and plasma environment and the results will be useful for the proposed missions to the Jovian system. It builds on previous papers, the most recent has now appeared in Icarus.

This new work, as the authors say, is not a unique solution since the data they compare to is limited, but the results are suggestive. The work indicates that simply adding a hot O2 component to their previous modeling was not sufficient to explain the dearth in their model electron densities, though how hot O2 might help was not made clear. But they showed that increasing the estimates of the atmospheric O2 column density and the electron ionization frequency would allow them to understand and model the available data.

This is all useful so that the work should be published. But was there a reason one thought the hot O2 might be important? It would seem to have, a priori, a small effect. Also having to wade through what is not useful (hot O2) to get to the point that one might need to boost the crude estimate of O2 density and the electron impact ionization frequency seemed an effort.

Energetic neutrals are produced in a region where the electron density was found to be underestimated, hence it seems reasonable to verify quantitatively their impact on the plasma density through simulations and to report it. In addition, the results obtained from the study of hot O_2 are relevant for the upcoming JUICE mission. In this context, measurements can be compared to our simulations, and they can be used as a validation tool for our model.

As correctly pointed out by the reviewer, hot O_2 turns out to be irrelevant for explaining the discrepancy between the ionospheric model and the PWS observations. As such, we moved the discussion of energetic neutrals (Section 2.2) to the appendix, achieving also a considerable reduction in the length of the main body of the manuscript.

A small paragraph was added to substitute Section 2.2 (lines 294-303):
"We used the collision scheme to simulate, through ad hoc simulations, the dynamics of energetic neutrals produced through charge-exchange with the ionosphere. As a result, we derived the first 3D maps for hot O_2, which was not included in the exospheric model of Leblanc (2017). The results of these simulations are presented in Appendix A. As it turns out, the inclusion of energetic neutrals at high altitudes does not address the issue of underestimated plasma density along the Galileo trajectory. Nonetheless, the results from this study are relevant for comparing with future in situ measurements by the Particle Environment Package (PEP) on board the JUICE spacecraft."

The work should be published, but the manuscript seems much longer than necessary to make their points. I started noting some awkward statements (even one of the first sentences: lines 30- 31 ---are Ganymede's ionospheric ions causing sputtering and the 'latter' is assessed?). Even later in lines 425 - 433 a single sentence would seem to do.

Line 30-31 [now lines 41-43] has been changed to: "...sputtering from Jovian magnetospheric ions and from Ganymede's ionospheric ions (the ionospheric contribution has been assessed for the first time in Carnielli et al., submitted)".

In regard to the content in lines 425-433 [now lines 347-355], we find it all to be useful for the reader, and that it cannot be merged into a single sentence. Hence, we left it as it is.

Therefore, I strongly support publishing this after the authors make an effort to simplify and shorten the writing. For instance, since their calculations are related to those in their previous papers they could rely more on those papers. If hot O2 is not important they could address that more efficiently and get to the point of what is important sooner.

See our response to the first point.

Again, the work is good and should be published. This referee does not need to see it again.

Reviewer 2

This manuscript represents a very valuable contribution to an improved understanding of Ganymede's exosphere and plasma environment. It provides an independent constraint on the exospheric density, which is presently poorly constrained. It makes good sense that an improved understanding of the electron density would provide a better constraint on the exospheric density implied by the observations, it was explicitly mentioned by Hall et al. that a future improved understanding of the electron density would allow a much more accurate determination of the exospheric density. I have no major issues with the paper, and recommend it be published largely as is, after the authors take into consideration the one point below.

The authors cite the Carlson et al. 1973 "detection" of Ganymede's exosphere. However, I am not aware of anyone who thinks that Ganymede actually has an exosphere with pressure of a microbar, including Carlson. This paper has been largely discounted over time. The observations are poor, they are made in the visible, no plausible exosphere was discussed or modeled based on these observations, the only suggestion for a possible atmospheric constituent was nitrogen. These same types of observations were used by the same authors to rule out an exosphere on Io, which we now know well has a much more robust atmosphere than that of Ganymede. This claimed detection by Carlson et al. was superseded by the Broadfoot et al. 1979 non-detection and upper limit, which was much more stringent and based on much higher quality data. I would urge the authors to give a more complete history of the detections and non-detections, i.e., I suggest that you also cite the Broadfoot paper and its upper limit, which is inconsistent with the Carlson "detection." I would also recommend that you compare your new constraint on the exospheric density/pressure with these two historical constraints, in addition to comparing it with the Hall et al. results.

We have modified the introduction as follows (lines 27-39):

"Quantitative observations of Ganymede's exosphere started with Carlson et al. (1973) who exploited a stellar occultation by Ganymede to observe the red and blue regions of the visible spectrum. These observations effectively marked the discovery of a thin gas envelope around the moon, indicating the presence of an atmosphere with a surface pressure greater than about 10^{-3} millibar.

With the arrival of Voyager 1 at Jupiter in 1979, the onboard UVS spectrometer took advantage of an occultation of K Centauri by Ganymede to make limb observations in the UV spectrum range. These new measurements placed an upper limit of $2x10^{-8}$ millibar - or equivalently $1.5x10^9$ cm^{-3} - for the surface density of suspected dominant species like H_2O and O_2 (Broadfoot et al., 1981), which is a factor of 10^{-5} lower than the lower limit derived by Carlson et al. (1973) and which appears to be unrealistically high."

As for comparing our constraint on the exospheric density with Broadfoot et al. (1981), we have added a few sentences in the conclusions, in the same paragraph where we compare with previous estimates by Hall et al. and exospheric models (lines 550 - 555):

“The comparison with Broadfoot et al. (1981) is limited since they only provided an upper limit for the exospheric surface density 1.5x10^9 cm^{-3}, and not for the column density. Considering only this value and assuming the same scale height as in the model of Leblanc et al. (2017), the required exospheric configuration is within the limit derived by Broadfoot et al. (1981).”

I'd also suggest that in future the authors consider using their modeling to predict the auroral emission morphology, and then compare this with the auroral observations, which provide another excellent constraint on the modeling. This is outside the scope of the present paper but would be a valuable additional test of the models.

Thank you for the suggestion. We plan to address this in a future study.

Highlights

- Ganymede O_2 exosphere should be denser than previously anticipated. While previous observation-driven and model-based estimates found a column density of the order of 10^{14} cm^2, we find that this value should exceed 10^{15} cm^2.
- We have improved the ionospheric model of Carnielli et al. (2019) by adding collisions between ion and neutral species, and found that this process has an appreciable effect on the ion distribution only at altitudes below 200 km.
- Through test particle simulations, we generated the first 3D maps of density and velocity of energetic O_2 in Ganymede's exosphere, a population that will be assessed by the JUICE-PEP instrument. In this context, these 3D maps will be useful for interpreting in situ data.

Constraining Ganymede's neutral and plasma environments through simulations of its ionosphere and Galileo observations

G. Carnielli[a,*], M. Galand[a], F. Leblanc[b], R. Modolo[c], A. Beth[a], X. Jia[d]

[a] *Department of Physics, Imperial College London, SW7 2AZ, London, United Kingdom*
[b] *LATMOS/IPSL, CNRS, Sorbonne Université, UVSQ, Paris, France*
[c] *LATMOS/IPSL, UVSQ Université Paris-Saclay, UPMC Univ. Paris 06, Guyancourt, France*
[d] *Department of Climate and Space Sciences and Engineering, University of Michigan, Ann Arbor, MI 48109-2143, USA*

Abstract

Ganymede's neutral and plasma environments are poorly constrained by observations. Carnielli et al. (2019) developed the first 3D ionospheric model aimed at understanding the dynamics of the present ion species and at quantifying the presence of each component in the moon's magnetosphere. The model outputs were compared with Galileo measurements of the ion energy flux, ion bulk velocity and electron number density made during the G2 flyby. A good agreement was found in terms of ion energy distribution and bulk velocity, but not in terms of electron number density.

In this work, we present some improvements to our model (Carnielli et al., 2019) and quantitatively address the possible sources of discrepancy found in the electron number density between the Galileo observations and our ionospheric model. We have improved the ion model by developing a collision scheme to simulate the charge-exchange interaction between the exosphere and the ionosphere. We have simulated the energetic component of the O_2

*Principal corresponding author:
Email address: gianluca.carnielli10@imperial.ac.uk (G. Carnielli)

population, which is missing in the exospheric model of Leblanc et al. (2017) and added it to the original distribution, hence improving its description at high altitudes. These improvements are found to be insufficient to explain the discrepancy in the electron number density. We provide arguments that the input O_2 exosphere is underestimated and that the plasma production acts asymmetrically between the Jovian and anti-Jovian hemispheres. In particular, we estimate that the O_2 column density should be greater than 10^{15} cm^{-2}, i.e., higher than previously derived upper limits (and a factor 10 higher than the values from Leblanc et al. (2017)), and that the ionization frequency from electron impact must be higher in the anti-Jovian hemisphere for the G2 flyby conditions.

Keywords: Ganymede, Ionospheres, Jupiter, satellites, Satellite, atmospheres

1. Introduction

Quantitative observations of Ganymede's exosphere started with Carlson et al. (1973), who exploited a stellar occultation by Ganymede to observe the red and blue regions of the visible spectrum. These observations effectively marked the discovery of a thin gas envelope around the moon, indicating the presence of an atmosphere with a surface pressure greater than about 10^{-3} millibar.

With the arrival of Voyager 1 at Jupiter in 1979, the onboard UVS spectrometer took advantage of an occultation of K Centauri by Ganymede to make limb observations in the UV spectrum range. These new measurements placed an upper limit of 2×10^{-8} millibar – or equivalently 1.5×10^{9} cm^{-3} – for the surface density of suspected dominant species like H_2O and O_2 (Broadfoot et al., 1981), which is inconsistent with Carlson et al. (1973) being a factor of 10^{-5} lower than their derived lower limit.

The major exospheric sources are sublimation of the icy surface in the subsolar region, sputtering from Jovian magnetospheric ions and from Ganymede's ionospheric ions (the ionospheric contribution has been assessed for the first time in Carnielli et al., submitted). Despite the confirmation of the presence of an exosphere by remote-sensing observations, little is known with certainty regarding its properties. The presence of O and O_2 has been inferred from UV emissions at 1304 Å and 1356 Å measured remotely by the Hubble Space Telescope (Hall et al. (1998); Feldman et al. (2000); McGrath et al. (2013); Molyneux et al. (2018)). The 3D distribution of these species around the moon is poorly constrained, and our current knowledge builds primarily on exospheric models that have been developed in the past 12 years (e.g., Marconi (2007); Turc et al. (2014); Plainaki et al. (2015); Shematovich (2016); Leblanc et al. (2017)). These models made assumptions regarding the sputtering and sublimation fluxes, and validated their outcome by comparing the column density of O_2 with that derived by Hall et al. (1998) from OI FUV emissions.

Hall et al. (1998) estimated an O_2 column density in the range 10^{14} – 10^{15} cm^{-2}. Exospheric models found that O_2 dominates in the region of open magnetic field lines (or everywhere, in the case of the model of Leblanc et al. (2017), in the case of a low ice sublimation rate in the subsolar region). We argue that the estimate of Hall et al. (1998) was made on the basis of strong assumptions regarding the electron distribution. Hall et al. (1998)

derived the O_2 column density from the observed UV emissions assuming a hypothetical distribution of electrons. They made use of the electron number density recorded during the Galileo G1 and G2 flybys, those which occurred closest to the moon and contained primarily electrons from Ganymede's ionosphere rather than the Jovian magnetosphere (Carnielli et al., 2019). Their estimate assumed that all electrons ($\sim$100 cm^{-3} at the surface) are able to excite auroral emissions on O_2, i.e., that all electrons are energetic enough to do so. The dissociative excitation of O_2 has an energy threshold around 14–15 eV and the associated cross-section peaks near 100 eV (Kanik et al., 2003). Hence, ionospheric electrons, which dominate inside the magnetosphere (Carnielli et al., 2019), would need to undergo significant acceleration, and the way this would occur is not clear, as argued also by Eviatar et al. (2001a). However, a recent modeling study by Zhou et al. (2019) suggests that energization through magnetic reconnection at the upstream magnetopause can contribute as much as 40% of the energy flux required to produce the observed auroral emissions. Hall et al. (1998) rightly had to make assumptions regarding the electron distribution in the absence of in situ measurements near the separatrix region, i.e., where the emissions dominate. However, the closest approach for G1 and G2 occurred inside the northern Alfvén wing, where the electron distribution is likely to differ significantly from that near the boundary between open and closed magnetic field lines. As a consequence, the distribution used by Hall et al. (1998) might not be the suitable one in order to retrieve the O_2 column density from the OI FUV emissions. A way to reproduce the observations in a more realistic way would be to reduce the density of exciting electrons, which implies to increase that of O_2. In this work, we present independent arguments to show that, in fact, the O_2 exosphere should be denser than what was previously estimated and modeled.

Ganymede's ionosphere is also poorly constrained in terms of observations, which come only from the Galileo mission. Using radio occultation measurements, Kliore (1998) derived an upper limit of 4000 cm^{-3} for the electron number density at the surface. Along the G1 and G2 flybys, the PWS instrument on board Galileo measured the electron number density (primarily of ionospheric origin near closest approach), while the PLS instrument recorded the ion bulk flow velocities and ion energy spectra (Frank et al., 1997). For the G2 flyby, the flow was originally interpreted by Barth et al. (1997) as escaping hydrogen ions. However, this was later reinterpreted as a flow of oxygen ions by Vasyliūnas and Eviatar (2000), which is supported by the MHD simulation results of Jia et al. (2009), and a combination of both species by Paty et al. (2008), who argued, using the outcome from their MHD simulations, that only H^+ would be detected by the PLS instrument. More recently, Collinson et al. (2018) re-analyzed the PLS data from the G1 and G2 flybys, showing different fits for different assumed ion masses. Remarkably, for the G2 flyby none of the fits can match the electron density profile – which, assuming quasi-neutrality, should equal to the total ion density – derived from PWS and reported in Eviatar et al. (2001b). In summary, the ionospheric composition is a subject of debate.

Simplistic efforts to characterize the ionosphere have been made by Eviatar et al. (2001b) and Cessateur et al. (2012). More recently, we have developed the first 3D multi-species test particle model of Ganymede's ionosphere (Carnielli et al., 2019). In this model, ions are generated from the ionization of the neutral exosphere, whose 3D configuration is taken from the recent model of Leblanc et al. (2017); they move in the electromagnetic field environment modeled by Leclercq et al. (2016) or Jia et al. (2009), and the distribution moments (number density, bulk velocity, temperature) are collected on a 3D spherical grid. Both the model of Eviatar et al. (2001b) and Carnielli et al. (2019) found the ionosphere to be dominated by O_2^+ near the surface, including the location of closest approach of the Galileo spacecraft during G2. This is supported by our finding that the major ion species observed by PLS was O_2^+ (Carnielli et al., 2019). A good agreement of our modeled output was found with the Galileo data in terms of ion energy distribution. A discrepancy, however, was found in terms of electron number density, with an underestimation of the modeled density compared to the measured one by more than one order of magnitude. Considering that the energy distribution agrees well with observations, which suggests that the fields describe well the field configuration at the time of the G2 flyby, it was concluded that the input exosphere is the likely cause for the discrepancy.

In this work, we have made improvements to the ionospheric model and quantitatively addressed the possible sources of discrepancy between our model and observations in terms of electron number density. Our original ionospheric model, presented in Carnielli et al. (2019), did not include collisions between ions and neutrals. Collisions with the neutral exosphere lead to a transfer of kinetic energy from the ionosphere to the exosphere, resulting in an increased ion density closed to the surface. In addition, the input exosphere from the model of Leblanc et al. (2017) did not include the energetic O_2 component, whose source is charge-exchange with ionospheric ions; but which ultimately is also a source of ionospheric ions. To address these limitations, we have developed a collision scheme to simulate the interaction between the major ions and neutral species in the atmosphere, i.e., O_2^+, O^+ and O_2. From this scheme, we have derived a production map for energetic O and O_2 and simulated the dynamics of these populations with ad hoc simulations. As it turns out, these changes do not improve the comparison of the electron number density along the G2 flyby. Hence, we have investigated further the discrepancy by searching for an appropriate physical configuration, in terms of exospheric densities and ionization sources, with which the simulation results are consistent with the Galileo observations.

The paper is organized as follows. Section 2 describes the collision scheme and its effect on the outputs of the ionospheric model. In Section 3 we describe an unsuccessful attempt to fit the Galileo observations by adapting only the new configuration of the neutral exosphere, while in Section 4 we describe a successful attempt by adapting both the new configuration of the neutral exosphere and the ionization sources. Finally, Section 5 summarizes and discusses the results achieved in this study.

2. Improvements to the ionospheric model

2.1. Modeling ion-neutral interactions

2.1.1. Motivation

Carnielli et al. (2019) showed that ionospheric particles interact more frequently with the neutral exosphere close to the surface (below approximately 200 km), where the timescale of collisions between ionospheric particles and neutral species is comparable to that of transport (cf. Figure 6 and Section 3.4.2 in Carnielli et al., 2019). However, they did not include collisions as they estimated that the ion production rate from charge-exchange is negligible compared to those from photo- and electron-impact ionization. In fact, the collision process, by slowing down the ion, could have an effect on the ionospheric configuration to the extent that it leads to an increased amount of time spent inside the cell, leading to an increased ion number density. Despite providing a measure of how important collisions can be in terms of production rate, the study presented in Carnielli et al. (2019) could not determine the effects that collisions would have on the dynamical evolution of the test-particle trajectories and on the distribution moments maps. In addition, in a denser exosphere (as later discussed in Section 3) collisions become even more important to consider. Regardless of the exospheric configuration, including collisions leads to a more realistic simulation, thus we have developed a collision scheme that has been integrated into the original model described in Carnielli et al. (2019).

2.1.2. Collision scheme

The interaction between ionized and neutral species involves momentum transfer collisions and charge-exchange reactions. Since in the exosphere modeled by Leblanc et al. (2017) O_2 is the dominant component (close to the surface where densities are highest and collisions matter), we have considered only this neutral species in the collision scheme. Banks (1966) showed that at energies above 0.5 eV, which applies to Ganymede's ionosphere, the neutral and ion species undergo charge-exchange rather than momentum transfer collisions. Due to the dominance of O_2^+ and O^+ in the ionosphere (Carnielli et al., 2019), combined with their higher cross-section for charge-exchange with O_2, we have considered only these two ion species in the collision scheme. More specifically, the following reactions have been considered:

$$O_2 + O^+_{2,\mathrm{f}} \longrightarrow O^+_2 + O_{2,\mathrm{f}} \tag{1}$$

$$O_2 + O^+_{\mathrm{f}} \longrightarrow O^+_2 + O_{\mathrm{f}}, \tag{2}$$

where 'f' means fast. Charge-exchange between O_2 and O^+ has been considered also with Jovian O^+ ions, which constitute the majority of the bulk plasma sheet population (Neubauer, 1998) (see Section 5.1.1 in Carnielli et al. (2019) for a description of how Jovian ions were simulated).

Ions undergo charge-exchange with the neutral exosphere at all times at a given rate, $\nu^{cx}_{i,n}$, given by:

$$\nu^{cx}_{i,n} = n_n \sigma^{cx}_{i,n}(E)|\vec{v}_i - \vec{v}_n|, \tag{3}$$

where $\sigma^{cx}_{i,n}$ is the energy-dependent charge-exchange cross-section between neutral species n and ion species i, $\vec{v}_n$ and $\vec{v}_i$ their velocity, and n_n the local number density of n. The values for the energy-dependent cross-section with O_2 were taken from Stebbings et al. (1963) for O_2^+ and from Lindsay and Stebbings (2005) for O^+. The energy E refers to the relative kinetic energy between i and n. In the simulations, i always moves significantly faster compared to n, thus E refers simply to the kinetic energy of i and $\vec{v}_n$ is neglected, i.e., n is assumed to be stationary in the charge-exchange process.

Mathematically, the probability of charge-exchange (CX) occurring between time t and $t + \Delta t$, which is an indication of the fraction of test particle (hereafter referred to as 'MP') that exchanges an electron with the neutral

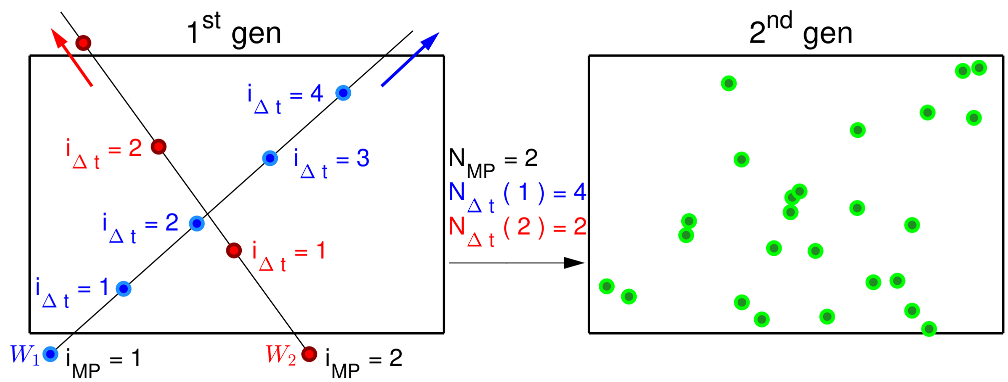

Figure 1: Schematic diagram of the collision scheme. See text for a full explanation.

population, can be formulated by the following expression (Modolo et al., 2016):

$$p_{i,n}^{CX}(t \rightarrow t + \Delta t) = 1 - \exp^{-\nu_{i,n}^{cx}\Delta t}. \qquad (4)$$

The probability tends to be 0 for a very short time interval and increases in time proportionally to the reaction frequency $\nu_{i,n}^{cx}$, defined in Equation 3.

Figure 1 shows a schematic diagram of the collision scheme. In the simulations, test particles are generated from ionization of the neutral exosphere, or belong to the plasma sheet in the case of Jovian O^+ ions. We refer to these test particles as belonging to the 1^{st} generation. These correspond to those simulated also in the collisionless scenario. The left panel in Figure 1 shows a simplified exospheric grid cell (the rectangle) crossed by two test-particle trajectories belonging to the 1^{st} generation. The trajectories look straight in order to simplify the visualization, but in the simulation they are determined by the local electromagnetic field. Each test particle has an index 'i_{MP}' and a weight $W_{i_{MP}}$, indicating the number of physical particles represented.

At each timestep $i_{\Delta t}$, the test particle interacts with the local neutral environment, and its weight is reduced by an amount equal to the fraction $p^{CX}_{i_{\Delta t},i_{MP}}$ of MP that undergoes charge-exchange. This approach has been implemented previously by Modolo et al. (2016) and validated by Chanteur et al. (2009) and Koutroumpa et al. (2012). As the particle's weight is reduced at each timestep k by $(1-p^{CX}_{k}, i_{MP})$, its weight loss at $i_{\Delta t} \geq 2$ is:

$$W_{lost}(i_{\Delta t}) = W_{i_{MP}} p^{CX}_{i_{\Delta t},i_{MP}} \prod_{k=1}^{i_{\Delta t}-1} (1 - p^{CX}_{k,i_{MP}}). \tag{5}$$

The lost weight is deposited and accumulated in the exospheric grid cell. In the left panel of Figure 1, the red particle ($i_{MP} = 2$) deposits part of its weight at steps $\mathrm{i}_{\Delta\mathrm{t}} = 1$ and $\mathrm{i}_{\Delta\mathrm{t}} = 2$ (only when it is found inside the exospheric grid cell). Instead, the blue particle ($i_{MP} = 1$) deposits part of its weight at four iterations. At the first iteration inside the cell, i.e., $\mathrm{i}_{\Delta\mathrm{t}} = 1$, the red particle deposits a weight equal to $p^{CX}_{1,2} W_2$. The first sub-index refers to the iteration inside the cell, and the second index corresponds to the value of i_{MP}. After the first iteration, the MP's weight is reduced to $(1 - p^{CX}_{1,2})W_2$. At $\mathrm{i}_{\Delta\mathrm{t}} = 2$ the particle deposits a weight equal to $p^{CX}_{2,2}(1 - p^{CX}_{1,2})W_2$, and so on. The same applies to the blue particle, which reduces its weight at the four iterations during which it is found inside the exospheric cell. The total weight deposited can be expressed as follows:

$$W = \sum_{i_{MP}=1}^{N_{MP}} W_{i_{MP}} \left(p^{CX}_{1,i_{MP}} + \sum_{i_{\Delta t}=2}^{N_{\Delta t}(i_{MP})} p^{CX}_{i_{\Delta t},i_{MP}} \prod_{k=1}^{i_{\Delta t}-1} (1 - p^{CX}_{k,i_{MP}}) \right), \tag{6}$$

where N_{MP} is the number of test particles of the 1^{st} generation that cross the exospheric cell and $N_{\Delta t}(i_{MP})$ is the number of iterations spent by test particle i_{MP} inside the cell. The lost weight is then reassigned to a newly-born test particle, belonging to the 2^{nd} generation, which represents those stationary ions produced from charge-exchange. These are initialized with a null velocity (because neutrals are assumed at rest) and a weight determined by the accumulated charge-exchange in the cell. To have sufficient statistics, typically 50 of such MPs are produced in each cell at random positions. These MPs – shown as green in the right panel of Figure 1 – can undergo further charge-exchange or, for the last generation considered, can be assumed to be collisionless. The user defines the number of generations to be simulated. In theory, charge-exchange should be calculated with each generation of MPs, which would make the simulation indefinitely long. In practice, MPs in higher generations carry only a fraction of the weight compared to the parent MPs, therefore calculating the charge-exchange process for new generations becomes progressively irrelevant. We have verified that including five generations is enough for the convergence of the results.

2.2. Effects of collisions

The physical effect of charge-exchange in the ionospheric model is to slow down test particles. If it takes more effort for the test particle of a species compared to another to be accelerated again by the fields after the collision, then we expect the effect of collisions to be more visible for this species. Due to the higher inertial mass of O_2^+ compared to O^+, the effects of collisions were seen to be more important for the former species. Thus, here only the effects of collisions for O_2^+ are discussed.

Figure 2 shows the average – over latitude and longitude – O_2^+ number density obtained from simulations with and without collisions (red and blue curves, respectively). For the simulation with collisions, the green curve shows the contribution from the first generation, and the orange curve that

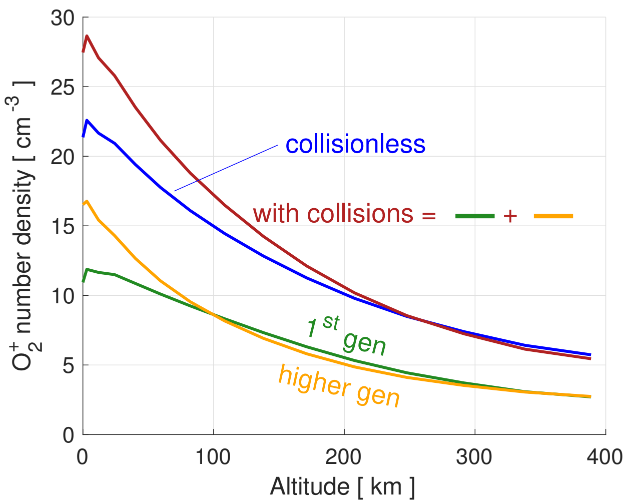

Figure 2: Average (over latitude and longitude) O_2^+ number density as a function of altitude. Blue curve: Simulation without collisions. Red curve: Simulation with collisions. Green curve: Contribution from the first generation of test particles. Orange curve: Contribution from higher generations. The sum of the green and orange curves corresponds to the red curve.

from higher generations (in total, 5 generations were simulated): the sum of these two contributions represents the total contribution (red curve). Overall, the effect of collisions is to boost the O_2^+ number density close to the surface, where the charge-exchange frequency is highest. The energetic O_2 population provides a negligible contribution to the charge-exchange due to the low number density compared to the thermal population close to the surface. This applies also to the number density profile of energetic O_2 from Marconi (2007), which is 3 orders of magnitude higher compared to that found by our simulations. Below approximately 260 km ($\approx 0.1\ R_G$), collisions lead to an increased number density (up to 30% near the surface), while at higher altitudes they result in a slight decrease. Although Figure 2 shows the average value over all latitudes and longitudes, this trend is seen everywhere around Ganymede, including the Alfvén wings and the equatorial region (not shown).

The density increase below 260 km is associated with the larger time spent in this region by test particles from higher generations, i.e., those which underwent charge-exchange with O_2: close to the surface, the particles from higher generations (orange curve) dominate in terms of number density compared with those from the first generation (green curve). Physically, this means that upon collision, test particles tend to stay near the surface and eventually impact instead of escaping, like those which did not undergo any collision. In contrast, at altitudes above 260 km the simulation with collisions yields a slightly lower density compared to the collisionless simulation. Such a migration towards the surface can be explained in terms of the electric field from the MHD model, whose radial component, on average, points towards the surface (not shown) at altitudes below 260 km. In other words, due to

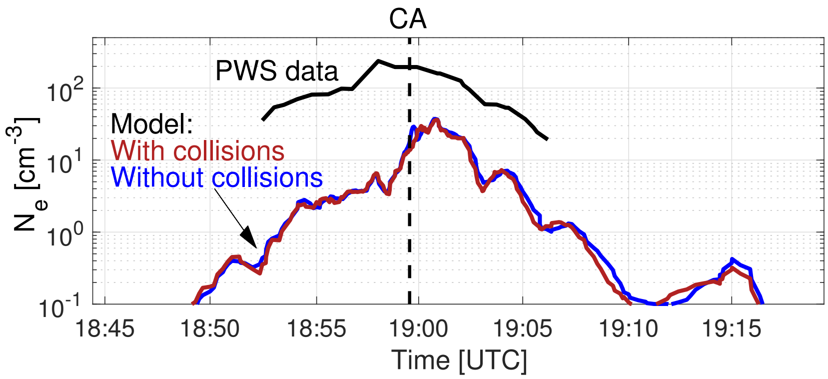

Figure 3: Electron number density along the G2 flyby as measured by: PWS (black), a simulation without collisions (blue) and one with collisions (red).

energy conservation MPs that are created with null velocity from charge-exchange accelerate to a region of lower electric potential, i.e., closer to the surface, compared to their parent MP which is at the same physical position but has higher kinetic energy.

Figure 2 indicates that at 260 km, which corresponds to the distance of closest approach of the Galileo spacecraft during the G2 flyby, charge-exchange has almost no effect on the number density of O_2^+, at least on average. This is demonstrated by Figure 3, which shows the electron number density along the G2 flyby for the two simulations (blue curve for the one without collisions and red curve for the one with collisions). The red and blue curves almost overlap each other, confirming that collisions have no appreciable effect over this altitude range. For reference, the electron density measured by the PWS instrument is plotted in black.

We used the collision scheme to simulate, through ad hoc simulations, the dynamics of energetic neutrals produced through charge-exchange with the ionosphere. As a result, we derived the first 3D maps for hot O_2, which was not included in the exospheric model of Leblanc et al. (2017). The results of these simulations are presented in Appendix A. As it turns out, the inclusion of energetic neutrals at high altitudes does not address the issue of underestimated plasma density along the Galileo trajectory. Nonetheless, the results from this study are relevant for comparing with future in situ measurements by the Particle Environment Package (PEP) on board the JUICE spacecraft."

In summary, we conclude that including the energetic component of the O_2 population, therefore increasing its density at high altitudes, and including collisions in the ionospheric model are not sufficient to explain the discrepancy in number density between the model and observations.

3. Optimizing Ganymede's exosphere in light of Galileo observations

Considering that the input electric and magnetic fields from the MHD model of Jia et al. (2009) provide a good description of the ion dynamics and lead to a good agreement with the observed ion energy spectrogram along the G2 flyby (Carnielli et al., 2019), and that collisions are insufficient to explain the order of magnitude gap between the modeled and observed electron number density, we have identified the neutral exosphere as a source of discrepancy.

In exospheric models, the ejection rate of neutral gases from Ganymede's icy surface has either been fine-tuned to ultimately have the O_2 column density match with that estimated by Hall et al. (1998) (Leblanc et al., 2017), or estimated by combining laboratory data on photolysis and radiolysis rates with ion fluxes measured by the EPD instrument during the close Galileo flybys (e.g. Shematovich (2016); Marconi (2007)), or again calculated by dynamically simulating the impact of Jovian ions on the moon's surface and making assumptions regarding the sputtering yields (Plainaki et al., 2015). However, the yield values have not been confirmed by direct measurements. Different models implemented ejection rates which differ by more than one order of magnitude (e.g. Plainaki et al. (2015) and Leblanc et al. (2017)). The source of uncertainty comes primarily from the sputtering yield associated with the ion impact, which depends on several parameters, many of which related to the detailed surface structure, which are not easy to estimate and replicate with laboratory experiments.

The discrepancy with observations found by the ionospheric model hints that the ejection rates used in the model of Leblanc et al. (2017), which is a driver of the ionospheric model, could be underestimated. Teolis et al. (2009) showed that the ejection rate of O_2 is not directly correlated to the incoming flux of energetic ions impacting the surface; they showed that O_2 is formed within the surface and accumulates before being released into the atmosphere, i.e., it is not sputtered immediately. As a consequence, the ejection rate of this species cannot either be easily quantified from simulations of plasma impacting Ganymede's surface. Estimates usually assume that the production of H_2/O_2 is a constant fraction of the H_2O ejected (like assumed by Leblanc et al. (2017)). However, Teolis et al. (2017) showed that, in fact, the relative yield is highly dependent on the energy of the impacting ion. Bearing in mind that the O_2 ejection rate is poorly constrained, we have

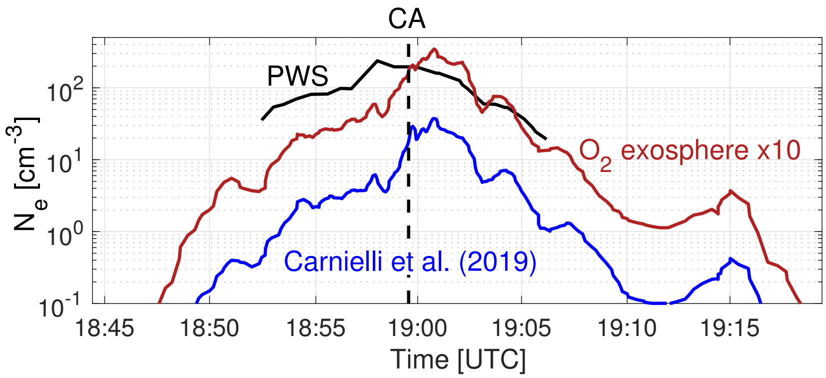

Figure 4: Electron number density along the G2 flyby as recorded by: the PWS instrument (black curve), an ionospheric simulation with the input exosphere from the model of Leblanc et al. (2017) (blue curve), and an ionospheric simulation run with the same exosphere boosted by a factor of 10 (red curve).

assessed how the discrepancy in electron number density along the G2 flyby varies in relation to a change of the O_2 distribution.

To increase the ion production rate we multiplied by 10 the O_2 distribution derived by Leblanc et al. (2017). This corresponds to assuming that the dynamics of molecules is exactly like the one simulated by Leblanc et al. (2017), but the ejection rate is increased by a factor of 10. Due to the lack of constraints for the ejection rate and the poor constraints on the column density, we argue that a boost by a factor of 10 is possible. This would bring the mean column density of O_2, the only "observational constraint", to 2.44×10^{15} cm^{-2}, which is just a factor of 2 higher than the upper limit estimated by Hall et al. (1998).

The electron density along the G2 flyby that results from an ionospheric simulation using this boosted configuration is plotted in red in Figure 4, while the blue curve shows the one obtained from an ionospheric simulation using the original exospheric configuration of Leblanc et al. (2017). Note that the red curve almost corresponds to the blue curve shifted upward by one order of magnitude. Even with the O_2 density increased by a factor of 10, collisions still leave almost unaffected the ionospheric configuration along the G2 flyby, and only near closest approach some differences are noticed. For the boosted exosphere case, there is a good match with PWS data in the outbound leg of the flyby, but there is still a discrepancy in the inbound leg, with the simulated density still lower compared to the measured values. This indicates that if the O_2 exosphere is considered as the only cause for the discrepancy, then the density of neutral species must be further increased in the region where test particles crossing the spacecraft trajectory in the inbound leg are produced. O_2^+ test particles crossing the Galileo G2 trajectory in the inbound leg are produced in the anti-Jovian hemisphere, while those crossing in the outbound leg are primarily produced in the Jovian-facing hemisphere (not shown). In order to have the electron number density match also in the inbound leg of the flyby, the O_2 distribution would have to be locally increased by an additional factor of 4 in the anti-Jovian hemisphere, at least in the region of open magnetic field lines. In the exospheric model of Leblanc et al. (2017), a longitudinal asymmetry features in the equatorial region due to the accumulation of O_2 in the afternoon side due to Ganymede's rotation, but such an asymmetry amounts to less than a factor of 2, and is confined to the low latitudes. Elsewhere, O_2 distributes homogeneously as it does not stick to the surface. Being unable to find a physical justification to explain a factor of 4 difference in the O_2 number density in the polar regions, we have concluded that the O_2 distribution alone cannot justify the discrepancy.

It could be argued that O_2 might not be the only underestimated neutral species in the model of Leblanc et al. (2017). Indeed, the exospheric model could not reproduce the Ly-α emission lines observed by the Galileo UV spectrometer, which suggests that the H exosphere simulated might be underestimated. However, we have checked that boosting the density of all neutral species by 10 yields the same result as boosting only the O_2 distribution for the purpose of matching the electron number density along the G2 flyby because the latter species largely dominates the plasma composition (see Figure C.13 in Carnielli et al. (2019)). Moreover, the other neutral species do not accumulate in the surface like O_2, hence their ejection rate is more constrained than that of O_2.

4. Electron-impact ionization frequency revisited

If the exosphere is not responsible alone for the discrepancy between the observed and modeled electron densities along the G2 trajectory, the only other option left is the ionization frequency. In the ionospheric model, the neutral exosphere is ionized by solar EUV radiation and Jovian magnetospheric electrons. On the one hand, the photo-ionization process is derived from the solar flux, which is known with a good level of confidence. On the other hand, the electron-impact ionization frequency, which is an order of magnitude larger than the photo-ionization frequency (Carnielli et al., 2019), is less certain and potentially too strong assumptions have been made in the ionospheric model. Here, we review in more detail the way the electron-impact ionization frequency was calculated (Section 4.1). Then, we present results of simulations that implemented different electron-impact ionization frequencies in different regions (Section 4.2), showing how this can significantly improve the comparison with observations.

4.1. Observations of energetic electrons

The results presented thus far have been obtained from simulations in which the ionization frequency from electron-impact was calculated using the electron distribution outside Ganymede's magnetosphere and set constant everywhere outside the region of closed magnetic field lines (see Section 3.1.2 in Carnielli et al., 2019). Figure 5 (top) shows the data from Scudder et al. (1981) we used to obtain the electron intensity along the G2 flyby in the energy range 12–5000 eV. The blue and yellow curves indicate the electron distribution functions recorded, respectively, by Voyager 1 and 2 in 1981 during plasma sheet crossings at two different locations inside Jupiter's magnetosphere: one at 12.87 R_J (blue) and the other at 18.4 R_J (yellow). The green curve shows the profile interpolated at Ganymede's orbital distance, at 15.4 R_J. The interpolation was done linearly as an approximation. To interpolate the distribution at energies below 20 eV, the yellow curve was logarithmically extrapolated down to 12 eV.

The bottom panel of Figure 5 shows the electron intensity as a function of energy. The blue and red curves show measurements made during the G2 flyby, for which there is a good match in the overlapping energy range. The profile obtained from the conversion of the green curve on the top panel is shown by the curve of the same color in the bottom panel. For energies between 600 eV and 5000 eV, the slope of the green and blue profiles match well. The magnitude, however, is off by a factor of 2.8. This can be due to a multitude of reasons, including the fact that the measurements by Voyager

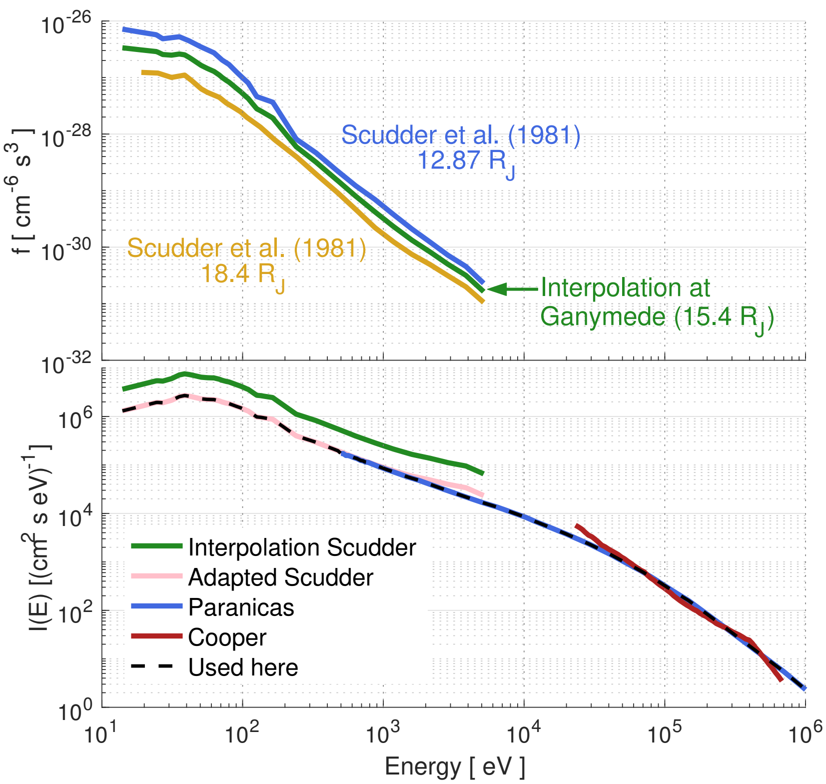

Figure 5: Top: Electron distribution function extracted from Scudder et al. (1981) (blue and yellow curves) at two distances from Jupiter in the magnetosphere and interpolated at Ganymede's mean orbital distance (gray curve). Bottom: Electron differential flux as a function of energy, outside the Jovian plasma sheet near Ganymede. Isotropy was assumed. The gray curve shows the flux computed from the distribution function in Scudder et al. (1981) adapted to Ganymede's orbital distance, the green curve shows the same but scaled to fit the blue curve in the shared energy range, the blue curve shows the flux presented in Paranicas et al. (1999), the red curve shows the flux presented in Cooper et al. (2001) and the dashed-black curve shows the combined flux adopted in our simulations.

1 and 2 were made when the spacecraft was inside the plasma sheet, while during the G2 flyby Galileo was above. In addition, the measurements of Voyager and Galileo were made at different epochs and positions, so it is very likely that the plasma conditions were not exactly the same between the two eras. As a consequence, the green profile was scaled down by a factor of 2.8 (pink curve) in order to fit the Galileo measurements. The re-scaling of the data is justifiable in the energy range where data is available from both sets of measurements. However, for energies below approximately 500 eV the scaling factor might not be necessarily correct across the whole energy range. Because the highest ionization cross-sections for electron impact are found near 100 eV, the calculated ionization frequency could be slightly different from what has been derived in combining these datasets together.

In the ionospheric model we have assumed a constant electron-impact ionization frequency over the region of open magnetic field lines at Ganymede because there is no usable data available for the electron phase-space distribution inside Ganymede's magnetosphere. Making such an assumption means that the effect of Ganymede's magnetosphere on the energetic electron population is ignored. Williams et al. (1998) presented count rates for the very energetic electrons (>15 keV) obtained by the PLS instrument along different flybys, including G2 (see Figure 1 in Williams et al., 1998). Although this dataset cannot be used directly to calculate the flux, it shows an asymmetry in the electron count rate between the inbound and outbound legs of the G2 flyby, which is not considered in the ionospheric model. It is true that the latter is more concerned with electrons in the energy range near 100 eV, but it is possible that such an asymmetry could feature at lower energies as well.

This asymmetry arises because the spacecraft travels through two different regions of Ganymede's magnetosphere. Before closest approach, it crossed a region with higher currents near the boundary between open and closed magnetic field lines. After closest approach, it traveled for a relatively long time (23 minutes) inside the northern Alfvén wing, where the plasma flow is more laminar (see Figure 7 in Carnielli et al. (2019)). The difference in the plasma behavior between these two regions is clearly visible in the energy spectra (cf. Figure 8b in Carnielli et al., 2019). The profile in Figure 1 of Williams et al. (1998) shows that before closest approach the instrument recorded a higher count rate. If that is the case for electrons with lower energies, it would explain the different slopes in the electron density profile recorded by the PWS instrument, which features a shallower slope in the inbound leg than in the outbound leg (see Figure 4). Hence, the ionization frequency could in fact be higher in the inbound leg of the G2 flyby. Moreover, the MHD model of Jia et al. (2008) found stronger currents in the anti-Jovian hemisphere compared to the Jovian-facing hemisphere for the G2 flyby conditions. Therefore, it is reasonable to argue that the actual ionization frequency could be different from what was originally assumed in our model and that the hemispheric asymmetry is indeed present.

4.2. Asymmetric electron-impact ionization frequency with boosted exosphere

We have found that in order to obtain a good agreement in the inbound part of the flyby, the O_2 distribution needs to be boosted by a factor of 10 and the electron-impact ionization frequency needs to be increased by a factor of 4 in the open magnetic field lines region around the subsolar longitude. This is plotted as the pink-shaded areas in Figure 6. The midday longitude is shown

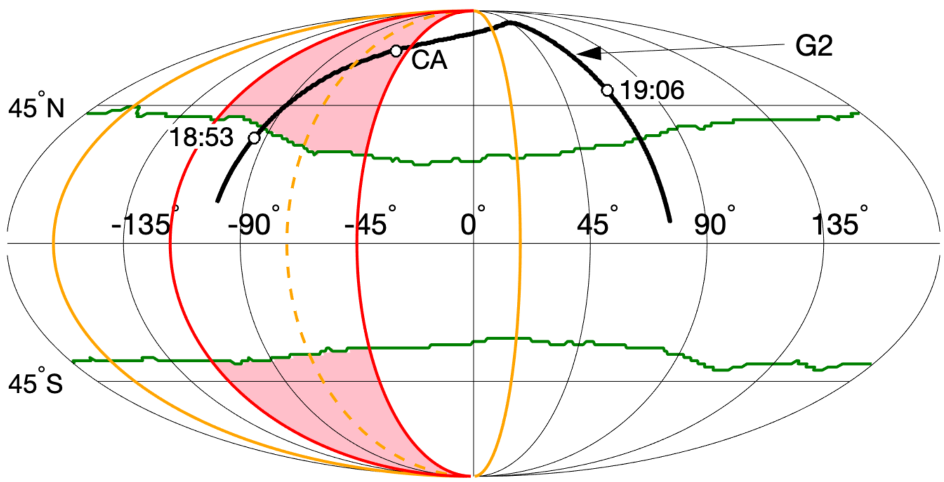

Figure 6: Mollweide projection of the G2 flyby trajectory (black line). In the longitudinal direction, 0° corresponds to the bisector of the leading hemisphere and 90° is towards Jupiter. The solid-orange line delimits the illuminated hemisphere and the dashed-orange line indicates the midday longitude. The pink-shaded areas, delimited by the red lines (at -117° and -45°), identify the region of open magnetic field lines where the electron-impact ionization frequency was increased. The green lines show the surface boundary between open and closed magnetic field lines.

by the dashed-orange line, while the illuminated hemisphere is delimited by the solid-orange line. Figure 6 shows also the G2 flyby trajectory and the locations from/to which the electron number density was reported in Eviatar et al. (2001b) (18:53 UTC and 19:06 UTC). 'CA' indicates the location of closest approach. In the simulation, test particles crossing the G2 trajectory in the inbound leg are produced primarily near the spacecraft location (not shown), which almost coincides with the pink-shaded area in the northern hemisphere. The longitude range delimiting the pink regions, spanning from -117° to -45°, is the one that was found leading to the best agreement with observations.

The electron number density (corresponding to the sum of all ion number densities) profile obtained by running the ionospheric model with this configuration is plotted in blue in Figure 7 (top panel). The fit with data (black curve) is very good over the inbound leg and the second half of the outbound leg, though the number density is overestimated by about a factor of 2–3 near closest approach. The middle and bottom panels of Figure 7 show, respectively, the measured and modeled ion energy spectrogram, the latter implementing the suitably boosted exosphere. Compared to the spectrogram in Figure 8 of Carnielli et al. (2019), the shape of the energy distribution is unchanged, and remains in agreement with observations. However, the ion intensity is increased by the exospheric and electron-impact frequency boost, and now matches the observed intensity (panel b).

Considering the approach applied to evaluate the ionization frequency from electron impact with the associated uncertainties, the factor of 4 increase in the electron-impact ionization frequency does not seem unrealistic,

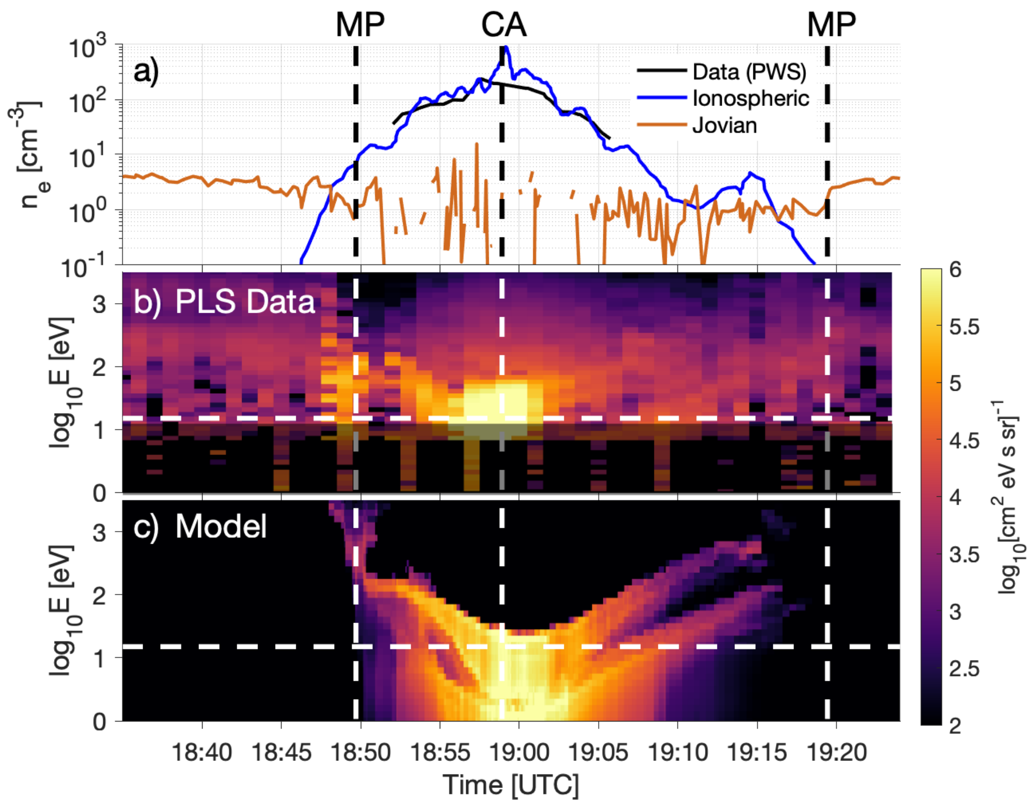

Figure 7: Top: Electron number density along the G2 flyby as a function of time as recorded by: the PWS instrument (black) and the ionospheric model (blue). The light brown profile shows the background Jovian ion density. Middle: Energy spectrogram as recorded by the PLS instrument. Bottom: Energy spectrogram as recorded by the ionospheric model. The white, dashed vertical lines indicate the times of magnetopause crossing (MP) and of closest approach (CA). The dashed, white horizontal lines in the middle and bottom panels show the upper energy limit below which the PLS dataset processing technique is considered as unreliable (see Carnielli et al. (2019) for more details). The simulation is driven by $n_{O_2} \times 10$ (compared to Leblanc et al., 2017) and an asymmetric electron-impact ionization frequency.

unlike the way in which the exosphere would have to be boosted if exospheric densities were the only source of uncertainty. Electron-impact ionization cross-sections are sensitive to the electron energy below 100 eV, and inside Ganymede's magnetosphere the electron energy distribution is affected by local processes, such as wave-particle interactions (Gurnett et al., 1996). Hence, it appears realistic to assume that the electron flux might be higher in correspondence to the strong currents at the Alfvén wings' boundaries and that the electron-impact ionization frequency could be boosted by as much as a factor of 4.

Although we find a good match in the electron number density along the G2 trajectory when boosting exospheric densities by a factor of 10 and the electron-impact ionization frequency by a factor of 4 in the anti-Jovian hemisphere, we acknowledge that this may not be the unique solution.

5. Conclusions

To date, Ganymede's neutral and plasma environments remain poorly constrained due to the lack of data. While waiting for new plasma, particle, and neutral data to come with the ESA JUICE mission, modeling efforts can be made to try improving our understanding of these physical environments and get the scientific community prepared for the mission. In this context, our ionospheric model is relevant to simulating the ion energy distribution and moments to be measured by PEP and RPWI instruments on board the JUICE spacecraft, and the modeling of hot O_2 presented in Appendix A is relevant to PEP as this population will be probed by its neutral channel.

Building from the original ionospheric model developed by Carnielli et al. (2019), we have investigated the neutral and plasma environments with the aim of finding a suitable configuration for the neutral exosphere and ionosphere in order to solve the discrepancy in the electron number density along the G2 flyby found by Carnielli et al. (2019). First, we have improved the ionospheric model by developing a collision scheme, simulating the energetic component of the input O_2 exosphere (absent in the exosphere modeled by Leblanc et al. (2017)) and adding it to the original exospheric O_2 distribution. Charge-exchange collisions lead to an increased ionospheric density close to the surface, but they cannot provide an explanation for the discrepancy between the model and Galileo observations in terms of electron number density. Hence, we have identified the neutral exosphere and the ionization frequency from electron-impact as the possible causes for this discrepancy. We have found that the O_2 exosphere should be denser than what has been published from observation-driven estimates (e.g., Hall et al. (1998), Feldman et al. (2000)) and those derived from previous exospheric models. More precisely, we find that the average O_2 column density should be $\sim 2.5 \times 10^{15}$ cm^{-2}, i.e., higher than the range of 10^{14}–10^{15} cm^{-2} derived by Hall et al. (1998) and a factor of 10 higher compared to the value found by the model of Leblanc et al. (2017). The comparison with Broadfoot et al. (1981) is limited since they only provided an upper limit for the exospheric surface density (1.5×10^9 cm^{-3}), and not for the column density. Considering only this value and assuming the same scale height as in the model of Leblanc et al. (2017)), the required exospheric configuration is within the limit derived by Broadfoot et al. (1981). As for the electron-impact ionization frequency, the discrepancy with Galileo observations can be solved if this parameter acts asymmetrically in the northern polar region with respect to the Jovian and anti-Jovian hemispheres, being about 4 times stronger in the latter (at least for the configuration of Ganymede during the G2 epoch). This asymmetry is supported by observations of the electron count rate by the EPD instrument (Williams et al., 1998). While there are uncertainties on these numbers, the key message is that only a boosted exosphere can realistically explain the underestimated electron density, and that the electron-impact ionization frequency likely acts asymmetrically between the Jovian and anti-Jovian hemispheres.

The next key step required to improve the quality of our study includes simulating the Jovian electron distribution inside Ganymede's magnetosphere. Having the 3D distribution of Jovian electrons inside the magnetosphere would allow to have a more realistic map of the ionization process of the neutral exosphere, which would improve the ionospheric model. Furthermore, it would allow to estimate more accurately the O_2 column density from the observed FUV emissions, since thus far too strong assumptions have been made for the exciting electrons producing these emissions.

6. Acknowledgments

Work at Imperial College London was supported by STFC of UK through a postgraduate studentship under grant ST/N000692/1. FL and RM acknowledge the support by the ANR HELIOSARES (ANR-09-BLAN-0223), ANR MARMITE-CNRS (ANR-13-BS05-0012-02) and by the "Système Solaire" program of the French Space Agency CNES. XJ acknowledges support by NASA's Solar System Workings program through grant NNX15AH28G.

Authors also warmly acknowledge the support of the IPSL data centre CICLAD for providing access to their computing resources.

Appendix A. Simulation of energetic neutrals

Leblanc et al. (2017) did not include any form of energetic neutrals in their model. These can be generated from the high energy tail of the distribution with which particles are ejected from the surface or from charge-exchange with ions, which can be from Ganymede's ionosphere or from Jupiter's magnetosphere. As the distribution of ionospheric ions was not available, Leblanc et al. (2017) neglected the charge-exchange process, obtaining an exosphere dominated by O_2 confined close to the surface. With the ionospheric model we have developed, it is possible to simulate this process and get a more realistic O_2 distribution at high altitudes.

The first step required to calculate the distribution of energetic neutrals is to determine their production rate as a function of position. This can be calculated while running the test particle code for the ion species selected for the charge-exchange process. We have considered Reactions (1) and (2), driven by ionospheric O_2^+ and ionospheric and Jovian O^+, which become, respectively, fast O_2 and fast O by reacting with O_2. At each iteration, a fraction of the test particle is neutralized by charge-exchange. The amount produced is recorded at each cell of the exospheric grid, together with the velocity and its spread. At the end of the simulation, 3D maps are generated for the production rate ($cm^{-3}\ s^{-1}$), average velocity, and average square velocity components of the energetic neutral species. Subsequently, a new simulation is run where the injected test particles are energetic neutrals in-

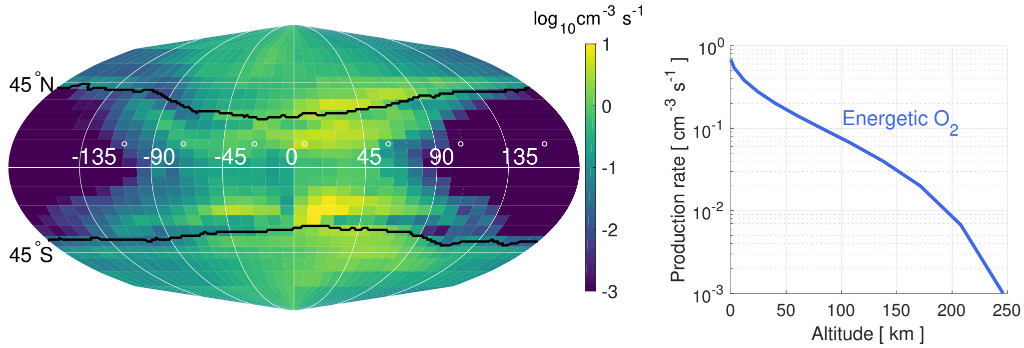

Figure A.8: Left panel: Map of O_2 production rate from charge-exchange with O_2^+ at the surface. In the longitudinal direction, 0° and 90°correspond to the bisectors of, respectively, the leading and Jovian-facing hemispheres. The black curves show the OCFB lines obtained from the MHD model of Jia et al. (2009). The color scale is logarithmic. Right panel: Average (over latitude and longitude) production rate of O_2 from charge-exchange with O_2^+ as a function of altitude.

stead of ionospheric ions. This is performed by loading the production map of energetic neutrals instead of the neutral exosphere. For such a simulation, in which test particles are electrically neutral, the only force felt is gravity, so the code behaves like an exospheric one. Like for the ionospheric simulation, test particles are followed either until they impact the moon's surface, or until they leave the simulation volume. Finally, 3D maps for the distribution of energetic neutral species are generated like for ionospheric ions.

According to our simulations, the most important charge-exchange reaction, in terms of occurrence, is that between O_2 and O_2^+, hence only results for this particular interaction are described here. However, the updated exospheric maps that have been subsequently used in our ionospheric model were produced considering also the interaction of O_2 with ionospheric and Jovian O^+. Figure A.8 shows the production rate of energetic O_2 produced from charge-exchange with O_2^+. The left panel shows the distribution of the production rate over the surface, while the right panel shows the average value (over latitude and longitude) as a function of altitude, which follows closely the O_2 variation in the model of Leblanc et al. (2017) (not shown). Over the altitude range in which collisions occur (within 0.1 $R_G \equiv 263$ km) the latitude-longitude distribution does not vary significantly in altitude, hence the two panels in Figure A.8 give a complete account of the energetic hot O_2 production map. The production rate at the surface peaks at about 10 $cm^{-3}s^{-1}$ and is found at low latitudes in the afternoon sector (between 0° and 90°, see left panel). This region corresponds to the maximum in exospheric O_2 density in the model of Leblanc et al. (2017), so collisions are more frequent. Although the O_2 exosphere is spread more or less constantly in the model of Leblanc et al. (2017), the left panel of Figure A.8 shows a clear asymmetry between the leading and trailing hemisphere in terms of production rate. This is because for the G2 flyby conditions ionospheric ions do not populate the trailing hemisphere at low altitudes (Carnielli et al., 2019), which reflects also in the production map of hot O_2. According to the ionospheric simulations, O_2^+ is produced mainly in the polar regions, and drifts toward the leading hemisphere at low latitudes, explaining the increased collision frequency, or equivalently the production rate of hot O_2 in this region.

Figure A.9 shows 2D maps of the number density of energetic O_2 in the XZ, YZ and XY planes (see figure caption for a description of the coordinate system). The maps have some similarities compared to that of O_2^+ (cf. Figure A.12 in Carnielli et al., 2019): the regions with higher number density

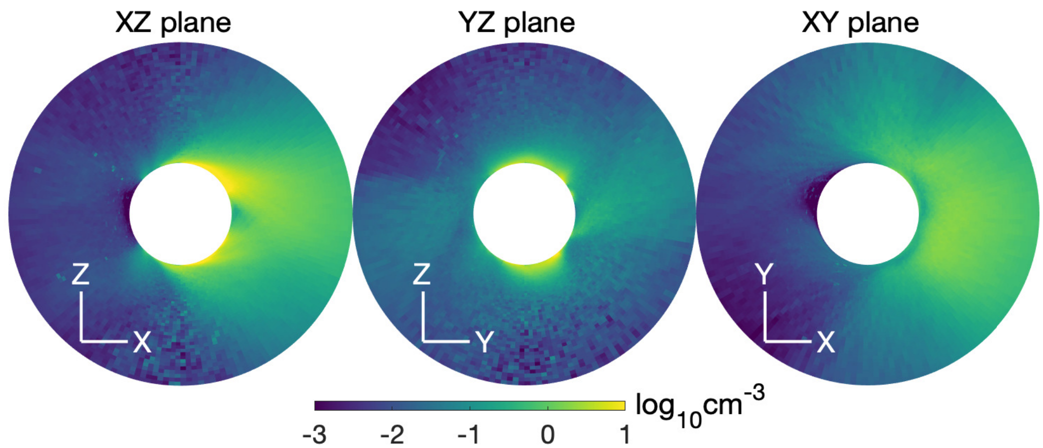

Figure A.9: Number density (in logarithmic color scale) of energetic O_2 resulting from charge-exchange with ionospheric O_2^+ in the XZ (left), YZ (middle) and XY (right) planes. X points in the direction of corotation of the Jovian plasma, Y points towards Jupiter and Z completes the right-handed coordinate system.

are the polar regions and the equatorial region in the leading hemisphere. Due to their neutrality, O_2 test particles are not tied to magnetic field lines and so do not mirror in the equatorial region. As a consequence, the rounded features seen in the O_2^+ density maps that reproduce the magnetic field lines at low latitudes are not present. However, 'jet-like structures' appear in this region. These form from energetic ions mirroring in the closed-field lines region. They get neutralized by charge-exchange and continue their journey almost in a straight line due to their high velocity.

The green profile in Figure A.10 shows the average altitude distribution obtained for hot O_2. This is how the O_2 distribution would extend if energetic neutrals were included in the model of Leblanc et al. (2017), for which the average altitude profile is plotted in blue. Above 250 km, the solid-blue curve decays in a physically unrealistic fashion. This problem is related to a lack

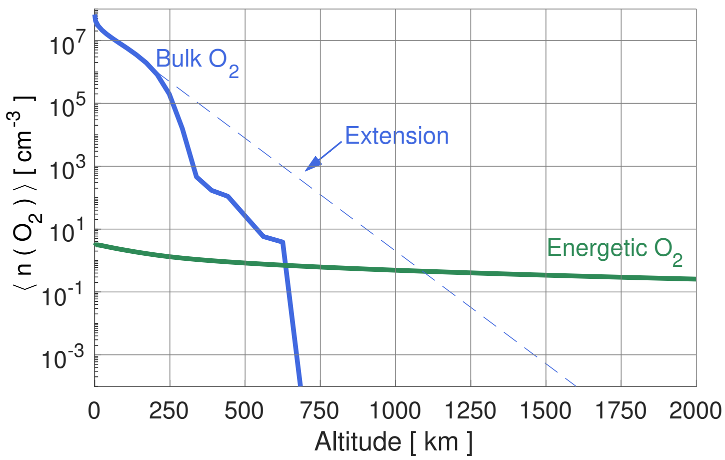

Figure A.10: Average number density as a function of altitude of the O_2 (solid-blue line) population from the exospheric model of Leblanc et al. (2017) and the energetic O_2 population produced through charge-exchange as simulated with the test particle code (green line). The dashed-blue line shows the extended profile of the bulk O_2 population in an ideal simulation scenario (i.e., not limited by particle statistics).

of statistics at high altitudes in the exospheric model, which are reached by neutrals in the energetic tail of the velocity distribution. Having a good statistic sampling for the energetic tail, without too many particle describing the core of the distribution, is numerically time consuming. The dashed-blue line is an extension of the blue profile and shows how the latter would theoretically extend to higher altitudes in the absence of particle statistics issues.

After deriving the distribution of hot O_2, the green profile in Figure A.10 was added to the blue profile, and the ionospheric model has been run with this new updated exosphere. Despite yielding an improvement to the model, the total production rates of O_2^+ and O^+ ions deriving from ionization of O_2 change negligibly since the neutral density at high altitudes is still 7 orders of magnitude lower compared to that close to the surface, hence the effects on plasma moments are negligible as well.

The results of our calculations regarding the altitude distribution of energetic O_2 can be compared to some extent with Marconi (2007), who also simulated charge-exchange collisions between O_2 and O_2^+. However, Marconi (2007) assumed an O_2^+ density considerably higher than that derived by our ionospheric model. In particular, Marconi (2007) assumed an exponentially decreasing density varying from 2000 cm^{-3} at the surface to 70 cm^{-3} at 0.1 R_G, which is at all altitudes about two orders of magnitude higher than in our model. In addition, the model of Marconi (2007) ejected neutral particles with a different energy distribution compared to Leblanc et al. (2017), which contains an energetic tail. These particles also populate the higher altitudes. As a result, Marconi (2007) found a density for the energetic O_2 population which is about 3 orders of magnitude higher compared to the profile shown in Figure A.10.

References

Banks, P., 1966. Collision frequencies and energy transfer. Ions. Planetary Space Science 14, 1105–1122. URL: `http://adsabs.harvard.edu/abs/1966P%26SS...14.1105B`, doi:`10.1016/0032-0633(66)90025-0`.

Barth, C.A., Hord, C.W., Stewart, A.I.F., Pryor, W.R., Simmons, K.E., McClintock, W.E., Ajello, J.M., Naviaux, K.L., Aiello, J.J., 1997. Galileo ultraviolet spectrometer observations of atomic hydrogen in the atmosphere at Ganymede. Geophysical Research Letters 24, 2147. URL:

http://adsabs.harvard.edu/abs/1997GeoRL..24.2147B, doi:10.1029/97GL01927.

Broadfoot, A.L., Sandel, B.R., Shemansky, D.E., McConnell, J.C., Smith, G.R., Holberg, J.B., Atreya, S.K., Donahue, T.M., Strobel, D.F., Bertaux, J.L., 1981. Overview of the Voyager ultraviolet spectrometry results through Jupiter encounter. Journal of Geophysical Research 86, 8259–8284. URL: http://adsabs.harvard.edu/abs/1981Sci...212..206B, doi:10.1029/JA086iA10p08259.

Carlson, R.W., Bhattacharyya, J.C., Smith, B.A., Johnson, T.V., Hidayat, B., Smith, S.A., Taylor, G.E., O'Leary, B., Brinkmann, R.T., 1973. An Atmosphere on Ganymede from Its Occultation of SAO 186800 on 7 June 1972. Science 182, 53–55. URL: http://adsabs.harvard.edu/abs/1973Sci...182...53C, doi:10.1126/science.182.4107.53.

Carnielli, G., Galand, M., Leblanc, F., Leclercq, L., Huybrighs, H.L.F., Jia, X., 2019. First 3D test particle model of Ganymede's ionosphere. Icarus URL: http://www.sciencedirect.com/science/article/pii/S0019103517307054, doi:10.1016/j.icarus.2019.04.016.

Cessateur, G., Lilensten, J., Barthélémy, M., Dudok de Wit, T., Simon Wedlund, C., Gronoff, G., Ménager, H., Kretzschmar, M., 2012. Photoabsorption in Ganymede's atmosphere. Icarus 218, 308–319. URL: http://adsabs.harvard.edu/abs/2012JSWSC...2A..16C, doi:10.1016/j.icarus.2011.11.025.

Chanteur, G.M., Dubinin, E., Modolo, R., Fraenz, M., 2009. Capture of solar wind alpha-particles by the Martian atmosphere. Geophysical Research Letters 36, L23105. URL: https://ui.adsabs.harvard.edu/abs/2009GeoRL..3623105C, doi:10.1029/2009GL040235.

Collinson, G., Paterson, W.R., Bard, C., Dorelli, J., Glocer, A., Sarantos, M., Wilson, R., 2018. New Results From Galileo's First Flyby of Ganymede: Reconnection-Driven Flows at the Low-Latitude Magnetopause Boundary, Crossing the Cusp, and Icy Ionospheric Escape. Geophysical Research Letters 45, 3382–3392. URL: https://ui.adsabs.harvard.edu/abs/2018GeoRL..45.3382C, doi:10.1002/2017GL075487.

Cooper, J.F., Johnson, R.E., Mauk, B.H., Garrett, H.B., Gehrels, N., 2001. Energetic Ion and Electron Irradiation of the Icy Galilean Satellites. Icarus 149, 133–159. URL: http://adsabs.harvard.edu/abs/2001Icar..149..133C, doi:10.1006/icar.2000.6498.

Eviatar, A., Strobel, D.F., Wolven, B.C., Feldman, P.D., McGrath, M.A., Williams, D.J., 2001a. Excitation of the Ganymede Ultraviolet Aurora. The Astrophysical Journal 555, 1013–1019. URL: http://adsabs.harvard.edu/abs/2001ApJ...555.1013E, doi:10.1086/321510.

Eviatar, A., Vasyliūnas, V.M., Gurnett, D.A., 2001b. The ionosphere of Ganymede. Planetary and Space Science 49, 327–336. URL: http://adsabs.harvard.edu/abs/2001P%26SS...49..327E, doi:10.1016/S0032-0633(00)00154-9.

Feldman, P.D., McGrath, M.A., Strobel, D.F., Moos, H.W., Retherford, K.D., Wolven, B.C., 2000. HST/STIS Ultraviolet Imaging of Polar Aurora on Ganymede. The Astrophysical Journal 535, 1085–1090. URL: http://adsabs.harvard.edu/abs/2000ApJ...535.1085F, doi:10.1086/308889.

Frank, L.A., Paterson, W.R., Ackerson, K.L., Bolton, S.J., 1997. Outflow of hydrogen ions from Ganymede. Geophysical Research Letters 24, 2151. URL: http://adsabs.harvard.edu/abs/1997GeoRL..24.2151F, doi:10.1029/97GL01744.

Gurnett, D.A., Kurth, W.S., Roux, A., Bolton, S.J., Kennel, C.F., 1996. Evidence for a magnetosphere at Ganymede from plasma-wave observations by the Galileo spacecraft. Nature 384, 535–537. URL: http://adsabs.harvard.edu/abs/1996Natur.384..535G, doi:10.1038/384535a0.

Hall, D.T., Feldman, P.D., McGrath, M.A., Strobel, D.F., 1998. The Far-Ultraviolet Oxygen Airglow of Europa and Ganymede. The Astrophysical Journal 499, 475–481. URL: http://adsabs.harvard.edu/abs/1998ApJ...499..475H, doi:10.1086/305604.

Jia, X., Walker, R.J., Kivelson, M.G., Khurana, K.K., Linker, J.A., 2008. Three-dimensional MHD simulations of Ganymede's magnetosphere. Journal of Geophysical Research (Space Physics) 113, A06212. URL: http://adsabs.harvard.edu/abs/2008JGRA..113.6212J, doi:10.1029/2007JA012748.

Jia, X., Walker, R.J., Kivelson, M.G., Khurana, K.K., Linker, J.A., 2009. Properties of Ganymede's magnetosphere inferred from improved three-dimensional MHD simulations. Journal of Geophysical Research (Space Physics) 114, A09209. URL: http://adsabs.harvard.edu/abs/2009JGRA..114.9209J, doi:10.1029/2009JA014375.

Kanik, I., Noren, C., Makarov, O.P., Vattipalle, P., Ajello, J.M., Shemansky, D.E., 2003. Electron impact dissociative excitation of O_2: 2. Absolute emission cross sections of the OI(130.4 nm) and OI(135.6 nm) lines. Journal of Geophysical Research (Planets) 108, 5126. URL: https://ui.adsabs.harvard.edu/abs/2003JGRE..108.5126K, doi:10.1029/2000JE001423.

Kliore, A.J., 1998. Satellite Atmospheres and Magnetospheres. Highlights of Astronomy 11, 1065. URL: https://www.cambridge.org/core/services/aop-cambridge-core/content/view/S1539299600019602.

Koutroumpa, D., Modolo, R., Chanteur, G., Chaufray, J.Y., Kharchenko, V., Lallement, R., 2012. Solar wind charge exchange X-ray emission from Mars. Model and data comparison. Astronomy & Astrophysics 545, A153. URL: https://ui.adsabs.harvard.edu/abs/2012A%26A...545A.153K, doi:10.1051/0004-6361/201219720.

Leblanc, F., Oza, A.V., Leclercq, L., Schmidt, C., Cassidy, T., Modolo, R., Chaufray, J.Y., Johnson, R.E., 2017. On the orbital variability of Ganymede's atmosphere. Icarus 293, 185–198. URL: http://adsabs.harvard.edu/abs/2017Icar..293..185L, doi:10.1016/j.icarus.2017.04.025.

Leclercq, L., Modolo, R., Leblanc, F., Hess, S., Mancini, M., 2016. 3D magnetospheric parallel hybrid multi-grid method applied to planet-plasma interactions. Journal of Computational Physics 309, 295–313. URL: http://adsabs.harvard.edu/abs/2016JCoPh.309..295L, doi:10.1016/j.jcp.2016.01.005.

Lindsay, B.G., Stebbings, R.F., 2005. Charge transfer cross sections for energetic neutral atom data analysis. Journal of Geophysical Research (Space Physics) 110, A12213. URL: http://adsabs.harvard.edu/abs/2005JGRA..11012213L, doi:10.1029/2005JA011298.

Marconi, M.L., 2007. A kinetic model of Ganymede's atmosphere. Icarus 190, 155–174. URL: http://adsabs.harvard.edu/abs/2007Icar..190..155M, doi:10.1016/j.icarus.2007.02.016.

McGrath, M.A., Jia, X., Retherford, K., Feldman, P.D., Strobel, D.F., Saur, J., 2013. Aurora on Ganymede. Journal of Geophysical Research (Space Physics) 118, 2043–2054. URL: http://adsabs.harvard.edu/abs/2013JGRA..118.2043M, doi:10.1002/jgra.50122.

Modolo, R., Hess, S., Mancini, M., Leblanc, F., Chaufray, J.Y., Brain, D., Leclercq, L., Esteban-Hernández, R., Chanteur, G., Weill, P., González-Galindo, F., Forget, F., Yagi, M., Mazelle, C., 2016. Mars-solar wind interaction: LatHyS, an improved parallel 3-D multispecies hybrid model. Journal of Geophysical Research (Space Physics) 121, 6378–6399. URL: https://ui.adsabs.harvard.edu/abs/2016JGRA..121.6378M, doi:10.1002/2015JA022324.

Molyneux, P.M., Nichols, J.D., Bannister, N.P., Bunce, E.J., Clarke, J.T., Cowley, S.W.H., Gérard, J.C., Grodent, D., Milan, S.E., Paty, C., 2018.

Hubble Space Telescope Observations of Variations in Ganymede's Oxygen Atmosphere and Aurora. Journal of Geophysical Research (Space Physics) 123, 3777–3793. URL: http://adsabs.harvard.edu/abs/2018JGRA..123.3777M, doi:10.1029/2018JA025243.

Neubauer, F.M., 1998. The sub-Alfvénic interaction of the Galilean satellites with the Jovian magnetosphere. Journal of Geophysical Research 103, 19843–19866. URL: http://adsabs.harvard.edu/abs/1998JGR...10319843N, doi:10.1029/97JE03370.

Paranicas, C., Paterson, W.R., Cheng, A.F., Mauk, B.H., McEntire, R.W., Frank, L.A., Williams, D.J., 1999. Energetic particle observations near Ganymede. Journal of Geophysical Research 104, 17459–17470. URL: http://adsabs.harvard.edu/abs/1999JGR...10417459P, doi:10.1029/1999JA900199.

Paty, C., Paterson, W., Winglee, R., 2008. Ion energization in Ganymede's magnetosphere: Using multifluid simulations to interpret ion energy spectrograms. Journal of Geophysical Research (Space Physics) 113, A06211. URL: http://adsabs.harvard.edu/abs/2008JGRA..113.6211P, doi:10.1029/2007JA012848.

Plainaki, C., Milillo, A., Massetti, S., Mura, A., Jia, X., Orsini, S., Mangano, V., De Angelis, E., Rispoli, R., 2015. The H_2O and O_2 exospheres of Ganymede: The result of a complex interaction between the jovian magnetospheric ions and the icy moon. Icarus 245, 306–319. URL: http://adsabs.harvard.edu/abs/2015Icar..245..306P, doi:10.1016/j.icarus.2014.09.018.

Scudder, J.D., Sittler, E.C., Bridge, H.S., 1981. A survey of the plasma electron environment of Jupiter - A view from Voyager. Journal of Geophysical Research 86, 8157–8179. URL: http://adsabs.harvard.edu/abs/1981JGR....86.8157S, doi:10.1029/JA086iA10p08157.

Shematovich, V.I., 2016. Neutral atmosphere near the icy surface of Jupiter's moon Ganymede. Solar System Research 50, 262–280. URL: http://adsabs.harvard.edu/abs/2016SoSyR..50..262S, doi:10.1134/S0038094616040067.

Stebbings, R.F., Turner, B.R., Smith, A.C.H., 1963. Charge Transfer in Oxygen, Nitrogen, and Nitric Oxide. Journal of Chemical and Physical Reference Data 38, 2277–2279. URL: http://adsabs.harvard.edu/abs/1963JChPh..38.2277S, doi:10.1063/1.1733961.

Teolis, B.D., Plainaki, C., Cassidy, T.A., Raut, U., 2017. Water Ice Radiolytic O_2, H_2, and H_2O_2 Yields for Any Projectile Species, Energy, or Temperature: A Model for Icy Astrophysical Bodies. Journal of Geophysical Research (Planets) 122, 1996–2012. URL: https://ui.adsabs.harvard.edu/abs/2017JGRE..122.1996T, doi:10.1002/2017JE005285.

Teolis, B.D., Shi, J., Baragiola, R.A., 2009. Formation, trapping, and ejection of radiolytic O_2 from ion-irradiated water ice studied by sputter depth profiling. The Journal of Chemical Physics 130, 134704–134704. URL: http://adsabs.harvard.edu/abs/2009JChPh.130m4704T, doi:10.1063/1.3091998.

Turc, L., Leclercq, L., Leblanc, F., Modolo, R., Chaufray, J.Y., 2014. Modelling Ganymede's neutral environment: A 3D test-particle simulation. Icarus 229, 157–169. URL: http://adsabs.harvard.edu/abs/2014Icar..229..157T, doi:10.1016/j.icarus.2013.11.005.

Vasyliūnas, V.M., Eviatar, A., 2000. Outflow of ions from Ganymede: A reinterpretation. Geophysical Research Letters 27, 1347–1349. URL: http://adsabs.harvard.edu/abs/2000GeoRL..27.1347V, doi:10.1029/2000GL003739.

Williams, D.J., Mauk, B., McEntire, R.W., 1998. Properties of Ganymede's magnetosphere as revealed by energetic particle observations. Geophysical Research Letters 103, 17523–17534. URL: http://adsabs.harvard.edu/abs/1998JGR...10317523W, doi:10.1029/98JA01370.

Zhou, H., Tóth, G., Jia, X., Chen, Y., Markidis, S., 2019. Embedded Kinetic Simulation of Ganymede's Magnetosphere: Improvements and Inferences. Journal of Geophysical Research 124. doi:10.1029/2019JA026643.